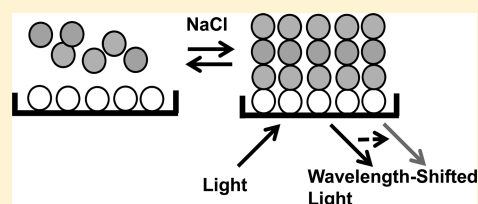


Functional Label-Free Assays for Characterizing the *in Vitro* Mechanism of Action of Small Molecule Modulators of Capsid Assembly

Latesh Lad,* Sheila Clancy, David Koditek, Melanie H. Wong, Debi Jin, Anita Niedziela-Majka, Giuseppe A. Papalia, Magdeleine Hung, Stephen Yant, John R. Somoza, Eric Hu, Chienhung Chou, Winston Tse, Randall Halcomb, Roman Sakowicz, and Nikos Pagratis

Gilead Sciences, 333 Lakeside Drive, Foster City, California 94404, United States

ABSTRACT: HIV capsid protein is an important target for antiviral drug design. High-throughput screening campaigns have identified two classes of compounds (PF74 and BI64) that directly target HIV capsid, resulting in antiviral activity against HIV-1 and HIV-2 laboratory strains. Using recombinant proteins, we developed a suite of label-free assays to mechanistically understand how these compounds modulate capsid activity. PF74 preferentially binds to the preassembled hexameric capsid form and prevents disruption of higher-order capsid structures by stabilizing capsid intersubunit interactions. BI64 binds only the monomeric capsid and locks the protein in the assembly incompetent monomeric form by disrupting capsid intersubunit interactions. We also used these assays to characterize the interaction between capsid and the host protein cleavage and polyadenylation specific factor 6 (CPSF6). Consistent with recently published results, our assays revealed CPSF6 activates capsid polymerization and preferentially binds to the preassembled hexameric capsid form similar to the small molecule compound, PF74. Furthermore, these label-free assays provide a robust method for facilitating the identification of a different class of small molecule modulators of capsid function.



The human immunodeficiency virus (HIV) continues to acquire resistance to currently administered antiretroviral drugs, and the rate of transmitted resistance is increasing.^{1,2} To overcome the emergence of drug resistance, there is a need for the discovery of new classes of antiretrovirals with distinct mechanisms for augmenting existing HIV treatment regimens. The capsid protein (CA) of HIV is such a target and has become a focus of antiviral research in recent years.³ During HIV virion maturation, CA is released from the Gag polyprotein by the viral protease.⁴ Upon entry of HIV particles into host cells, the CA core disassembles to allow reverse transcription and subsequent integration of the reverse-transcribed viral genome into the host DNA. The stability of the CA core and the corresponding rate of core disassembly are essential for successful viral infection,^{5,6} and mutations in CA protein have been shown to alter the infectivity, replication, and assembly of virions *in vivo*.⁷ Drugs that can modulate CA assembly or disassembly⁸ may represent new strategies for targeting an essential part in the life cycle of the HIV virus.

The CA protein is composed of two highly helical domains, the N-terminal domain (CA-NTD, residues 1–146) and the C-terminal domain (CA-CTD, residues 151–231), that are connected to each other by a short flexible linker.^{9–11} HIV-1 capsid lattices belong to a class of geometric structures called fullerene cones, which comprise hexagonal lattices with several pentagonal defects that allow the cones to close. Modeling studies of HIV-1 capsid reveal that the conically shaped lattice utilizes ~1500 CA monomers to assemble into a lattice of ~250 CA hexamers that is closed by the incorporation of

12 pentamers.^{7,12,13} Initial biochemical and genetic experiments suggested the existence of NTD–CTD interactions essential for capsid formation.^{7,14} These observations were confirmed using a high-resolution pseudoatomic model of full-length CA¹⁵ and an X-ray structure of a CA hexamer obtained by intersubunit disulfide cross-linking.¹⁶ These studies proposed a hexameric arrangement of CA monomers and revealed intermolecular contacts, including NTD–CTD and NTD–NTD interactions of neighboring subunits as well as CTD–CTD interactions that serve as bridges between hexamers. More recently, an atomic-level modeling of the HIV capsid was finally made possible by the solution of the X-ray structure of a CA pentamer that completes the structural determination of the components of the fully assembled capsid.¹⁷

High-throughput screening campaigns have recently identified two classes of small molecule inhibitors, PF74 and BI64 (Figure 1), both targeting CA with potent *in vitro* CA polymerization modulatory activity and antiviral potency.^{18,19} High-resolution structural studies reveal that both compounds bind to distinct sites located on the N-terminal domain of CA [CA-NTD (Figure 1)] and appear to differentially modulate *in vitro* capsid assembly (Figure 1). Biochemical CA assembly assays that utilize purified recombinant CA revealed that PF74 increased the rate of CA assembly whereas BI64 decreased the

Received: September 15, 2014

Revised: March 12, 2015

Published: March 16, 2015



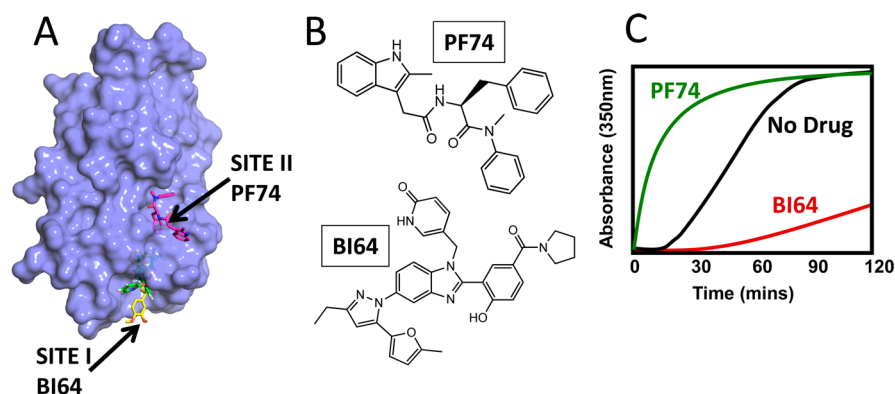


Figure 1. Binding sites of inhibitors and kinetics of HIV-1 CA assembly. (A) Superimposition of the BI64 CA-NTD cocrystal structure with PF74 bound to CA-NTD. (B) Chemical structures of compounds used in this study. (C) Detection of CA assembly by absorbance. In the presence of a high salt concentration, CA spontaneously polymerizes, causing a change in the optical density due to turbidity. PF74 (green trace) accelerated salt-induced CA assembly, whereas BI64 (red trace) inhibited salt-induced CA assembly.

rate of CA polymerization (Figure 1). Previously reported *in vitro* polymerization assays measure CA assembly by turbidity using an absorbance-based readout^{18,20} or a fluorescence-based readout using fluorescein-labeled deoxyoligonucleotide.¹⁹ Such assays are severely prone to compound and assay buffer composition interference. Herein, we report the development of a suite of label-free assays for mechanistically characterizing and improving our understanding of how PF74 and BI64 modulate CA assembly. We also used these label-free assays to characterize the interaction between CA and a cellular cofactor that facilitates viral infection. It has been shown that a 15-mer peptide, derived from the central proline rich domain of cleavage and polyadenylation specific factor 6 (CPSF6), containing a central FG motif is sufficient for binding to CA-NTD.²¹ CPSF6 is a host factor engaged in the processing of cellular precursor mRNA.²² It shuttles between the nucleus and cytoplasm and interacts via its C-terminal arginine/serine rich domain with karyopherin TNPO3, a nuclear import receptor. Several lines of evidence suggest that interaction between CA and CPSF6 facilitates viral infection.²³ Here we show that CPSF6 peptide modulates capsid assembly and exhibits a preference for binding to CA that is comparable to that of the small molecule modulator PF74.

EXPERIMENTAL PROCEDURES

Materials. Steptavidin (Sigma) and chemicals used for buffer preparation (Fisher) were of the highest analytical grade ($\geq 99\%$ purity) and used without further purification. Epic biochemical plates were purchased from Corning. OctetRed super streptavidin biosensors were purchased from ForteBio (Pall). Biacore biosensor chips were purchased from GE Healthcare (Piscataway, NJ). CPSF6 (CPSF6_{313–327} with sequence PVLFPQGPFQPPPLG) and F321N CPSF6 (F321N CPSF6_{313–327} with sequence PVLFPQGPPNGPPPLG) peptides were custom synthesized (Anaspec, CA). PF74, BI64, and CPSF6 peptide stock solutions were prepared in dimethyl sulfoxide (DMSO). All functional biochemical and biophysical assays were conducted in buffer containing 50 mM sodium phosphate (pH 7.5), 0.01% Tween 20, and 0.005% (v/v) Antifoam 204 with or without 0–2 M NaCl.

Construction of Wild-Type (WT) and Mutant CA (Hexamer) Expression Plasmids. A fragment encoding the 231 residues of wild-type (WT) CA protein was amplified via polymerase chain reaction (PCR) from the infectious HIV-1

cDNA plasmid, pLAI.2, obtained from J. M. Becket. The 5' PCR primer contains an NdeI cloning site and a codon for N-terminal methionine. The 3' PCR primer contains a stop codon and an XhoI cloning site. The amplified fragment was digested with NdeI and XhoI, gel-purified, and cloned into the NdeI and XhoI sites of the pET30a vector (catalog no. 70781, EMD BioSciences, La Jolla, CA). The quadruple mutant, 4Mut CA (A14C/E45C/W184A/M185A), was modified from WT CA by site-directed mutagenesis and was used to generate a stable engineered hexameric CA protein as previously described.^{16,24,25}

Protein Expression and Purification. Expression and purification of WT CA and CA hexamer proteins were performed as previously described.^{24,25}

Absorbance-Based Capsid Polymerization Assay. Polymerization reactions for WT CA were performed using a method similar to that described in a previous report.²⁰ WT CA was diluted 2-fold to a final concentration (0–80 μM) in buffer containing 50 mM sodium phosphate (pH 7.5) and 0.005% (v/v) Antifoam 204; 384-well plates (Costar catalog no. 3685) were prespotted with either DMSO or compound, and 10 μL of WT CA was dispensed into the assay plate using a BioTek μFill and incubated for 5 min at 25 °C. Polymerization was initiated by addition of 10 μL of buffer containing 50 mM sodium phosphate (pH 7.5), 4 M NaCl, and 0.005% (v/v) Antifoam 204. WT CA polymerization was monitored by measuring the sample absorbance at 350 nm for 12 h at 25 °C in an Envision plate reader (PerkinElmer). The final reaction conditions were 40 μM CA and various concentrations of inhibitors (starting concentration of 300 or 10 μM serially diluted 3-fold) in 50 mM sodium phosphate (pH 7.5), 2 M NaCl, 0.005% Antifoam 204, and 1% DMSO. Initial rates of the polymerization reaction were calculated from the slopes of the straight line fit to the linear portion of the kinetic curves of WT CA polymerization. The percent activity in the presence of compound was calculated as the percent of the initial rate in the presence of compound in comparison to the rate of the uninhibited polymerization reaction. IC_{50} and AC_{50} values were calculated from the fit of the compound dose–response curves to a four-parameter equation. All IC_{50} and AC_{50} values represent geometric mean values of a minimum of four determinations. These assays generally produced results within 3-fold of the reported mean.

Biosensor-Based Polymerization Assay. Biosensor-based WT CA polymerization and depolymerization assays

were performed on the Corning Epic System containing an integrated CyBio robotic liquid handling accessory. WT CA or streptavidin immobilization was accomplished by resuspending the protein (40–50 $\mu\text{g/mL}$) in 20 mM MES (pH 6.0) or 20 mM sodium acetate (pH 5.1), respectively, and adding 10 $\mu\text{L/well}$. The resulting Epic plates were incubated overnight at 4 °C and subsequently blocked with 150 mM borate buffer (pH 9.2) supplemented with 200 mM ethanolamine (Sigma) for 15 min and washed three times with assay buffer containing 0 mM NaCl. To the immobilized protein monolayer was added 15 $\mu\text{L/well}$ of resuspended WT CA in assay buffer containing 0 mM NaCl. A baseline read was taken; 15 $\mu\text{L/well}$ of assay buffer containing 4 M NaCl was added (final NaCl concentration in the assay of 2 M), and the resulting assay plate was read kinetically in the Epic reader. Once WT CA polymerization was complete, the assay plate was washed with assay buffer containing 2 M NaCl to remove any unbound protein. Another time point was taken followed by the addition of assay buffer (15 $\mu\text{L/well}$) containing 0 M NaCl. Addition of 0 M NaCl assay buffer stimulated depolymerization of the captured assembled WT CA polymers and was monitored kinetically using the Epic reader. Initial rates of the polymerization reaction were calculated from the slopes of the straight line fit to the linear portion of the kinetic curves of WT CA polymerization. The percent activity in the presence of compound or peptide (starting concentration of 300, 100 or 10 μM serially diluted 3-fold) was calculated as the percent of the initial rate in the presence of compound in comparison to the rate of the uninhibited polymerization reaction. IC_{50} and AC_{50} values were calculated from the fit of the compound dose–response curves to a four-parameter equation. All IC_{50} and AC_{50} values represent geometric mean values of a minimum of four determinations. These assays generally produced results within 3-fold of the reported mean.

Biacore Measurements. Surface plasmon resonance (SPR) measurements were performed on Biacore T100 (GE Healthcare) using CM5 research-grade sensor chips. Purified WT CA and assembled CA hexamer were minimally biotinylated at a ratio of one biotin molecule per molecule of either monomeric or hexameric capsid using EZ-Link Sulfo-NHS-LC-LC-Biotin (ThermoScientific, Barrington, IL). All binding experiments were performed in buffer containing 50 mM sodium phosphate (pH 7.5), 150 mM NaCl, and 0.01% (v/v) P20. CM5 sensor chips were preconditioned before neutravidin was immobilized over a range of 7000–9000 RU on all flow cells via standard amine coupling chemistry (GE Healthcare). Minimally biotinylated proteins were diluted in HEPES-buffered saline (pH 7.4) and injected over separate flow cells for varying periods of time until capture densities reached ~ 2500 RU for CA monomer and ~ 1300 RU for hexameric CA. Remaining free biotin-binding sites on the neutravidin surface were blocked with two 5 min injections of 0.5 mM EZ-Link-Amine-PEG2-Biotin at 30 $\mu\text{L/min}$. Kinetic measurements for capsid binding were performed by injecting buffer blank, peptide, PF74, and BI64 at various concentrations (starting concentration of 300 or 10 μM serially diluted 3-fold) over the captured CA proteins in the flow cells at a rate of 100 $\mu\text{L/min}$ for a 30 s association followed by a 60 s dissociation. At the end of each cycle, the injection needle and tubing were cleaned with a 50% DMSO wash. A five-point concentration series of DMSO (ranging from 0.5 to 1.5%) was injected at the beginning and end of the experiment to generate a calibration curve to correct for excluded volume effects.

Sensorgrams were double-referenced, corrected for solvent effects, and then fit using Scrubber version 2.0 (BioLogic Software, Campbell, Austria). Kinetic data were fit to a simple kinetic model. Fitted values were obtained for the association (k_{on}) and dissociation (k_{off}) rate constants as well as the equilibrium dissociation constant (K_{D}). When the off rate was too fast to be determined (i.e., $k_{\text{off}} > 1 \text{ s}^{-1}$), steady-state responses were also fit to a simple 1:1 binding isotherm to obtain values for K_{D} .

OctetRed Measurements. Samples or buffer was dispensed into 384-well tilted black bottom plates (Pall FortéBio Inc., Menlo Park, CA) at a volume of 90 $\mu\text{L/well}$. Super streptavidin biosensor (SSA) tips (Pall FortéBio, Inc.) were prewet with assay buffer [50 mM sodium phosphate (pH 7.5), 0.001% Tween 20, and 150 mM NaCl] to establish a baseline before protein immobilization. The biotinylated protein (WT CA and hexameric CA) was immobilized onto super streptavidin biosensors and then blocked with biocytin (Sigma). Kinetic measurements for compound or peptide binding were performed by dipping the biosensor into wells containing compound or peptide at various concentrations (starting concentration of 300, 30 or 10 μM serially diluted 3-fold) for 200 s followed by a 500 s dissociation by dipping biosensors into buffer-containing wells. Sensorgrams were double-referenced, corrected for solvent effects, and then fit using OctetRed user software (Pall FortéBio Inc.). The binding profile of each sample was summarized as an “nm shift” (the wavelength or spectral shift in nanometers), which represented the difference between the start and end of the kinetic cycle. Steady-state and kinetic responses were fit to a simple binding model to obtain values for association (k_{on}) and dissociation (k_{off}) rate constants and the equilibrium dissociation constant (K_{D}).

Isothermal Titration Calorimetry (ITC) Experiments. ITC experiments were performed using a VP-ITC instrument (Microcal, Northampton, MA) with a stirring speed of 490 rpm. Each analysis was performed in duplicate, and additional control experiments, including titration of inhibitor into buffer, were performed to measure the heat of dilution effects. CA protein was dialyzed into 50 mM sodium phosphate (pH 7.5) and 150 mM NaCl, and inhibitor was also dissolved in the same buffer. For each titration experiment, a 90 μM protein solution was degassed prior to being loaded into the ITC instrument. Inhibitor (30 μM) was injected with 30 portions of 10 μL with an injection syringe. Data were processed and analyzed using Origin (MicroCal).

■ RESULTS AND DISCUSSION

Characterization of PF74 and BI64 Using a Novel Biosensor-Based Polymerization Assay. Historical assays used to measure CA polymerization were absorbance-based, measuring turbidity,^{18,20} or had a fluorescence-based readout that employed a Gag fragment that spanned the CA and nucleocapsid regions and took advantage of the ability of nucleocapsid to bind tightly to fluorescein-labeled deoxyoligonucleotides.¹⁹ Unfortunately, these assays are severely prone to compound and assay buffer interference, and this prompted us to develop a novel label-free functional assay using the Corning Epic platform to understand how PF74 and BI64 modulate CA assembly. The Epic platform incorporates an evanescent waveguide biosensor within each well of its proprietary 384-well microplates. Direct binding or capture of ligands to target proteins immobilized onto the microplate well surface can be detected by exposing the waveguide to a broadband light

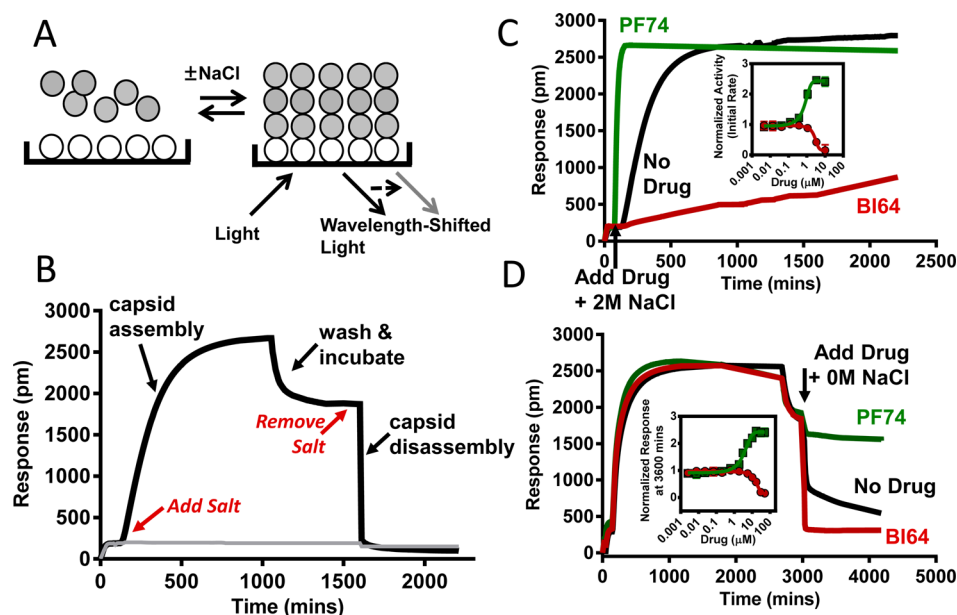


Figure 2. Epic label-free assay platform that can detect CA assembly and disassembly. (A) Schematic of the Epic technique for real-time measurement of the accumulation of mass on a biosensor. White circles represent monomeric CA immobilized on the biosensor surface. Gray circles are CA monomers in solution and in the presence of 2 M NaCl assembled on the immobilized CA monolayer. (B) Detecting salt-induced CA assembly and disassembly on the Epic label-free assay platform. The black trace represents the time course for salt-induced CA assembly and disassembly on an immobilized CA monolayer biosensor surface. The gray trace represents the time course for salt-induced CA assembly and disassembly on an immobilized streptavidin monolayer biosensor surface. (C) Modulation of CA assembly kinetics by PF74 (green trace) and BI64 (red trace) compared to no drug control (black trace). The inset shows the dose–response curves for CA activation by PF74 (green) and inhibition by BI64. The initial rate of CA assembly was calculated from the slope of the linear phase of each kinetic trace and normalized vs a no compound control and then plotted against each drug concentration. (D) Modulation of CA disassembly by PF74 (green trace) and BI64 (red trace) compared to the no compound control (black trace). CA was allowed to assemble, and unbound or unassembled CA was washed away. Compound was simultaneously added with no salt containing buffer to induce disassembly. The inset shows the dose–response curves for no salt-induced CA disassembly by PF74 (green) and BI64 (red). The response signal at a fixed time point of 360 min was normalized against the no compound control and then plotted vs each compound concentration.

source. The resulting resonant wavelength shift (measured in picometers) is proportional to the mass bound to the surface (Figure 2A). The Epic-based functional CA assay took advantage of CA's N-terminal and C-terminal ability to form intermolecular CA–CA interactions, leading to the formation of a tubular structure. The CA assembly reaction was achieved by first coating the biosensor surface with monomeric CA. The immobilized CA surface in each well acts to nucleate the assembly of stable CA tubes in the presence of high salt concentrations. The assembled CA was observed as a mass-dependent response (Figure 2A). A mass-dependent response was not observed in assay wells coated with streptavidin or buffer (Figure 2B).

Figure 2B shows the time-dependent mass change on an Epic biosensor surface for a salt-induced CA assembly and disassembly reaction. Addition of 2 M salt to monomeric CA at concentrations of $>10 \mu\text{M}$ activates CA assembly after an initial lag phase (~ 100 s), which is manifested by an increase in the magnitude of the response signal and plateaus at ~ 800 – 1000 s, indicating the end of the assembly reaction (Figure 2B). The lag phase, which has been observed using alternative assay formats, is postulated to be caused by the formation of assembly nuclei (trimers of CA dimers) and intermediates and is the rate-limiting step for the assembly reaction.²⁵ A minimum of $10 \mu\text{M}$ monomeric CA was used in the assay and is 4-fold lower than the protein concentration required in an absorbance-based readout.^{20,24} Unbound and unassembled species are washed away from the captured assembled product

at the end of the assembly reaction, and addition of salt-free buffer initiates CA disassembly and is monitored as a rapid decrease in the magnitude of the response signal (Figure 2B). The rate of CA polymerization was 0.0075 min^{-1} in the Epic assay compared to 0.039 min^{-1} in the absorbance-based turbidity assay. The difference in rates was due to the amount of protein used and the affinity of the CA–CA interaction. The K_D for CA–CA interaction is reported to be $20 \mu\text{M}$;²⁶ in the Epic assay format, we used $10 \mu\text{M}$ WT CA, whereas in the absorbance-based assay, we used a minimum of $40 \mu\text{M}$ to detect a measurable signal. Using a protein concentration below the K_D of the CA–CA interaction may result in an overall slower polymerization reaction with a weaker signal response (amount of polymerized CA). This may explain why the reaction time course for CA assembly in the absorbance-based assay was ~ 4 h whereas in the Epic assay it was ~ 16 h. Assembly experiments using higher protein concentrations ($40 \mu\text{M}$) resulted in complete assembly within 4 h using the Epic platform (data not shown). Aside from the higher sensitivity and the absence of fluorescent labels for detecting CA assembly and disassembly compared to previously reported assays, the Epic readout also allows the capture and integration of a stably formed CA polymer with small molecule druglike compounds.

To characterize the mode of action of PF74 and BI64 using the Epic-based CA functional assay, we first monitored the effect of PF74 and BI64 on the rate of CA assembly (Figure 2C). PF74 increased the rate of CA assembly and decreased the length of the lag phase ($AC_{50} = 0.89 \mu\text{M}$), whereas BI64

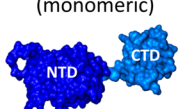
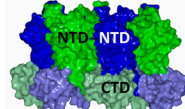
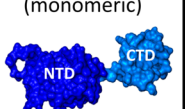
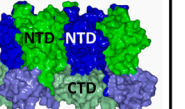
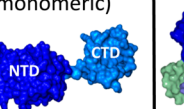

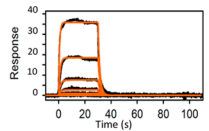
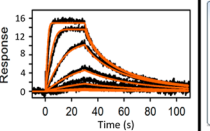
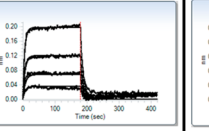
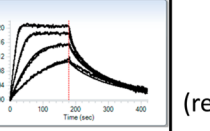
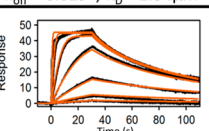
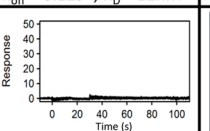
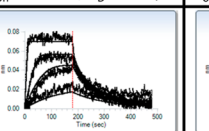
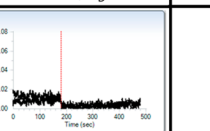
	Biacore (SPR) Binding Data		OctetRed (BLI) Binding Data		ITC Binding Data	
	WT CA (monomeric)	Hexamer CA	WT CA (monomeric)	Hexamer CA	WT CA (monomeric)	Hexamer CA
						
PF74	 $k_{on} = 4.64 \times 10^5 \text{ M}^{-1} \text{ s}^{-1}$; $k_{off} = 0.62 \text{ s}^{-1}$; $K_D = 1.34 \mu\text{M}$	 $k_{on} = 5.59 \times 10^6 \text{ M}^{-1} \text{ s}^{-1}$; $k_{off} = 0.12 \text{ s}^{-1}$; $K_D = 21 \text{ nM}$	 $k_{on} = 5.87 \times 10^4 \text{ M}^{-1} \text{ s}^{-1}$; $k_{off} = 0.11 \text{ s}^{-1}$; $K_D = 1.87 \mu\text{M}$	 $k_{on} = 1.57 \times 10^5 \text{ M}^{-1} \text{ s}^{-1}$; $k_{off} = 0.012 \text{ s}^{-1}$; $K_D = 78 \text{ nM}$	2.8 μM (reference (18))	120 nM (reference (27))
BI64	 $k_{on} = 4.50 \times 10^5 \text{ M}^{-1} \text{ s}^{-1}$; $k_{off} = 0.011 \text{ s}^{-1}$; $K_D = 25 \text{ nM}$	 detectable binding not observed	 $k_{on} = 2.98 \times 10^4 \text{ M}^{-1} \text{ s}^{-1}$; $k_{off} = 0.009 \text{ s}^{-1}$; $K_D = 83 \text{ nM}$	 detectable binding not observed	97 nM	detectable binding not observed

Figure 3. Binding of PF74 and BI64 to monomeric CA (contains both NTD and CTD) and hexameric CA analyzed by surface plasmon resonance (Biacore), bilayer interferometry (OctetRed), and isothermal titration calorimetry (ITC). All sensorgrams were fit to a 1:1 kinetic binding model, and all K_D values were calculated from the ratio of the k_{on} and k_{off} rate constants obtained from these fits. The highest compound concentration used was either 30 or 10 μM serially diluted 3-fold. In parentheses are cited references for ITC data.

decreased the rate of CA assembly ($\text{IC}_{50} = 4.2 \mu\text{M}$). This observation was consistent with the data reported from other assay formats.^{18,19,24} Because the Epic assay allowed us to capture a stable CA-polymerized product, we wanted to evaluate the effect of PF74 and BI64 on the rate of CA disassembly. For this experiment, we induced CA polymerization in the absence of compound using a high salt concentration and unbound or unassembled CA species was washed away. To the assembled CA product we added either PF74 or BI64 in the presence of salt-free buffer, and we monitored the rate of CA disassembly. To our surprise, PF74 appeared to prevent disruption of the polymerized CA product whereas BI64 appeared to accelerate disruption of polymerized CA compared to the no compound control trace (Figure 2D). These data suggest PF74 drives CA assembly to favor the formed assembled oligomer whereas BI64 favors CA in the unassembled form.

Analysis of Binding of PF74 and BI64 to Monomeric and Hexameric CA. To directly test the hypothesis that PF74 activates CA assembly to favor the assembled CA oligomer and BI64 favors CA in the unassembled monomeric form, we performed direct binding experiments using surface plasmon resonance (SPR), bilayer interferometry (BLI), and isothermal calorimetry (ITC) technologies to measure the affinity of PF74 and BI64 for WT monomeric CA and a CA hexameric protein engineered by intersubunit disulfide cross-linking of CA mutant A14C/E45C/W184A/M185A.¹⁶ The engineered hexameric protein used in our biophysical studies is formed by CA-NTD–NTD and CA-NTD–CTD interactions and represents one of the hexameric units found in the fully assembled conical HIV-1 CA lattice. For SPR-based measurements, we used a Biacore T100, and for the bilayer interferometry-based measurements, we used the OctetRed 384. Both platforms yield the binding affinity (K_D) and kinetic constants (k_{on} and k_{off}) for a biomolecular interaction; however, the bilayer interferometry technology does not utilize fluidics for a flow cell and as a result has no microfluidic constraints and is less

sensitive to sample composition (buffer reagents or compound properties). For binding experiments, WT monomeric CA and hexameric CA were minimally biotinylated and captured on either neutravidin-coated biosensor chips (SPR) or streptavidin sensor tips (BLI). The binding of PF74 and BI64 to the proteins was studied in buffer containing physiologically relevant salt concentrations (0.15 M NaCl). As shown in Figure 3, for both assay platforms PF74 was found to bind CA hexamer and CA monomer with a fast association rate, but a visibly slower dissociation rate was observed for the assembled hexamer compared to the CA monomer. The K_D values derived from these kinetic fits were 1.34 μM (Biacore) and 1.87 μM (OctetRed) for CA monomer and 21 nM (Biacore) and 78 nM (OctetRed) for the CA hexamer protein. This finding that PF74 binds a CA form with a K_D of <100 nM explains why its potency in infectivity experiments is significantly higher than its reported affinity.¹⁸ A very different binding signature against the two CA proteins was observed for BI64 compared to PF74. BI64 showed negligible binding to the assembled hexamer protein with an estimated affinity of >10 μM (Biacore) and >30 μM (OctetRed), which were the highest concentrations of compound tested because of limited compound solubility (Figure 3). BI64 was found to bind to CA monomer with a K_D of 25 nM (Biacore) and 83 nM (OctetRed). Although the K_D values determined using the two assay platforms are comparable and consistent with lower-throughput methods such as ITC,^{18,27} the kinetics of association and/or dissociation report differences of >5-fold (Figure 3). The differences in the kinetic parameters between the Biacore and OctetRed are most likely due to the different configurations of the microfluidics. Biacore (SPR)-based platforms require ligands to flow over the target protein using a flow cell; on the other hand, OctetRed (BLI) utilizes a plate-based dip and read configuration, and dissociation is assessed by dilution. Collectively, the binding data summarized in Figure 3 clearly show that PF74 preferentially binds to the assembled CA hexamer whereas BI64 only appears to bind to CA monomers. These data

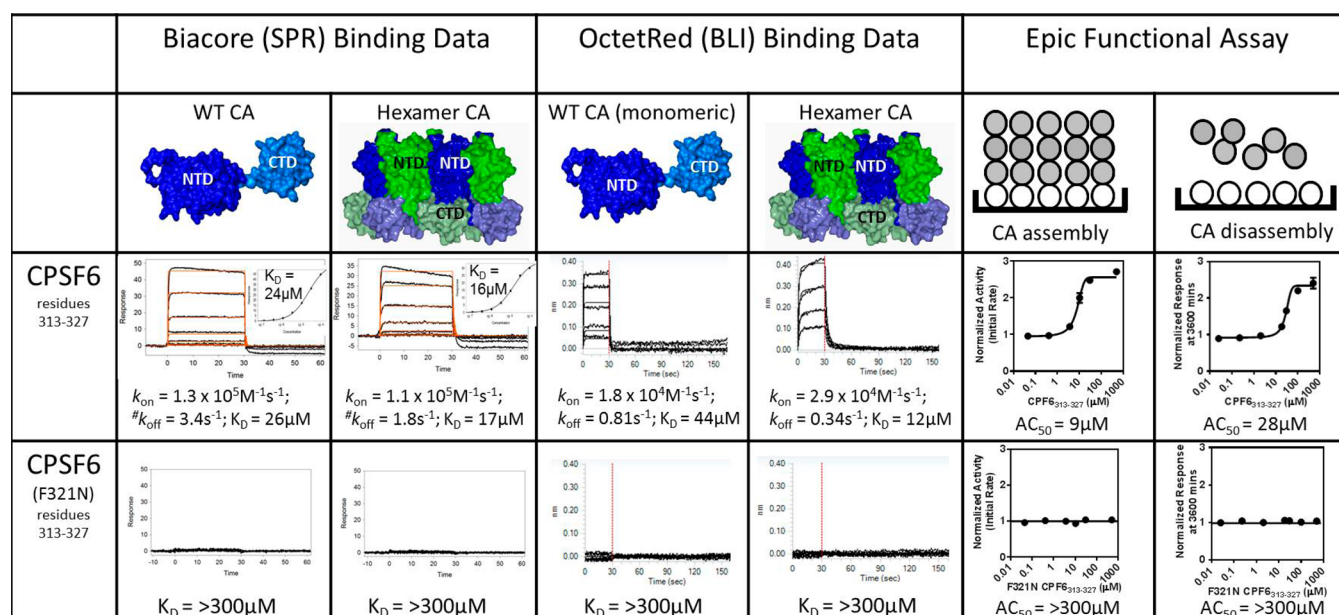


Figure 4. Characterization of a 15-mer peptide, derived from CPSF6, binding to HIV-1 CA using SPR (Biacore), BLI (OctetRED), and Epic assay platforms. Direct experiments examining binding of CPSF6 and F321N CPSF6 peptides to monomeric CA (contains both NTD and CTD) and hexameric CA were achieved by surface plasmon resonance (Biacore) and biolayer interferometry (OctetRed). All sensorgrams were fit to a simple kinetic model. Fitted values were obtained for the association (k_{on}) and dissociation (k_{off}) rate constants as well as the equilibrium dissociation constant (K_D). The number sign indicates that when the off rate was too fast to be determined ($k_{off} > 1 \text{ s}^{-1}$), steady-state responses were also fit to a simple 1:1 binding isotherm to obtain values for K_D (inset). The highest peptide concentration was 300 or 100 μM serially diluted 3-fold. Modulation of salt-induced CA was performed on the Epic platform. CPSF6 peptide-dependent activation of CA assembly was calculated from the slope of the linear phase of each kinetic trace, normalized against the no peptide control, and then plotted vs each peptide concentration. For CA disassembly, CA was allowed to assemble and unbound or unassembled CA was washed away. CPSF6 peptides were simultaneously added with no salt containing buffer to induce disassembly. Dose–response curves for no salt-induced CA disassembly were generated by plotting the normalized response signal at a fixed time point (360 min) vs CPSF6 peptide concentration.

correlate with the Epic-based functional assembly assay and are consistent with structural data related to the inhibitor-binding sites on CA. BI64 binds to an induced hydrophobic pocket at the base of the CA-NTD helical bundle.¹⁹ This pocket is located among α -helices 1, 2, 4, and 7 and is normally occupied by the aromatic side chain of Phe32 and His62 in the CA hexamer, pentamer, and monomer structures. Binding of BI64 repositions the flexible loop between helices 3 and 4 so that the loop conformation differs substantially from the apo-hexamer structure.¹⁶ All these changes would destabilize the CA-NTD–CTD interfaces that are required for the formation of higher-order assembled CA species. The high affinity of BI64 for monomeric CA in comparison to that for the preformed hexamer suggests BI64 stabilizes CA in the monomeric form and therefore inhibits CA assembly by preventing CA-NTD–CTD interactions. Furthermore, BI64 rapidly accelerates the disassembly of a polymerized CA product by disrupting CA-NTD–CTD interactions. The CA–CA interactions in the hexameric structure may hinder binding of BI64 but appear to present new interfaces for interaction that favor the binding of PF74. Unlike BI64, PF74 binds to a preformed pocket in CA-NTD between helices 4 and 7 and is distinct from the site targeted by BI64 (Figure 1), which results in a unique mechanism of action.¹⁸ The structure of PF74 bound to the preformed CA hexamer was recently published and revealed PF74 binds in a preformed pocket encompassing the NTD of one CA monomer and the CTD of another, which would allow modulation of intersubunit interactions and suggests the principal target of PF74 is the assembled capsid.²⁸ The structural and binding data for PF74 indicate that PF74 stabilizes

the CA-CTD–NTD intersubunit interactions, resulting in a more stable polymerized CA structure that cannot easily be disassembled.

Characterization of Binding of CPSF6 Peptide to HIV-1 Capsid Using Epic, BLI, and SPR Platforms. During the preparation of this work, there were two comprehensive studies characterizing the binding interaction of CA with the cellular host cofactor, CPSF6, that revealed it preferentially binds to the hexameric CA form and occupies an overlapping binding site to PF74.^{27,28} During the early stages of HIV infection, a number of complex series of steps occur that include translocation of the viral core through the cytosol, reverse transcription, CA uncoating, nuclear entry, and integration. To regulate these processes, a number of host factors have been identified, including CPSF6.^{23,29} CPSF6 is engaged in the processing of cellular precursor mRNA,²² shuttles between the nucleus and cytoplasm, and interacts via its C-terminal arginine/serine rich domain with karyopherin TNPO3, a nuclear import receptor. Depletion of CPSF6 inhibits infection of primary macrophages by revealing HIV-1 to the innate immune system.²⁹ It has been shown that a 15-mer peptide, derived from the central proline rich domain of CPSF6, containing a central FG motif is sufficient for binding to CA-NTD.²¹ Using the label-free assays described in this study, we characterized the binding and functional activity between CA and the CPSF6 peptide. Two CPSF6 peptides were tested, CPSF6_{313–327} and a mutated version of the peptide in which phenylalanine at position 321 was replaced with asparagine. The aromatic side chain of F321 forms extensive hydrophobic interactions with CA, indicating it is essential for CA binding, and the F321N mutation impairs

CPSF6 binding.²¹ Peptides were tested for binding to monomeric and hexameric CA. Binding to monomeric and hexameric CA was only observed with CPSF6_{313–327} and not F321N CPSF6_{313–327} (Figure 4). CPSF6_{313–327} showed an improved affinity for hexameric CA compared with that of monomeric CA (2–4-fold). In our studies, the interaction between CA and CPSF6_{313–327} is relatively weak, resulting in double-digit micromolar affinities (Figure 4). However, the affinities reported in this study and preferential binding for the hexameric CA form are consistent with binding data reported using alternative methods such as ITC, fluorescent polarization, and analytical ultracentrifugation.^{27,28} Further characterization of the peptide in the Epic functional assay revealed CPSF6_{313–327} increased the rate of CA assembly and decreased the rate of CA disassembly (Figure 4). F321N CPSF6_{313–327} showed no binding to monomeric or hexameric CA and was inactive in the functional Epic assay. This indicates the micromolar binding and potencies observed for CPSF6_{313–327} in the various label-free assays are specific. Lastly, comparison of the binding preference and mechanism of action in the Epic functional assay suggests CPSF6_{313–327} behaves like PF74. These data are consistent with the recently published structural and binding data that show that CPSF6_{313–327} preferentially binds to stabilized hexamers and occupies a preformed pocket encompassing the CA-CTD–NTD interface, which is the same binding site for PF74.^{18,21,27,28}

CONCLUSIONS

Capsid is the primary structural protein of HIV and plays a critical role in both late and early stages of the viral replication cycle. Functional studies of HIV-1 variants indicate that the proper assembly, morphology, and stability of the CA core are all essential for HIV-1 infectivity, and therefore, CA is considered an important therapeutic target that is currently unexploited clinically.^{5,6,30,31} As a drug discovery target, HIV-1 CA protein has been shown to be amenable to small molecule intervention with HTS campaigns identifying several classes of compounds that bind to distinct pockets on CA and modulate the *in vitro* rate of assembly and interfere with CA function in infected cells.^{18,19} In this study, we developed a suite of label-free assays to carefully characterize the primary mode of modulation of capsid assembly for two classes of small molecule inhibitors, PF74 and BI64, which were recently identified in HTS campaigns. The Epic-based assay described in this study is novel and allowed us to carefully characterize the effect of inhibitors on CA assembly and disassembly in real time without the use of labeled probes or historical detection methods that are sensitive to compound or buffer composition interference. Our assays showed that PF74 preferentially binds to the assembled (hexameric) form of CA and prevents disruption of higher-order CA structures by stabilizing CA-CTD–NTD interactions whereas BI64 locks CA in an unassembled (monomeric) form by disrupting CA-NTD–CTD interactions. These data are consistent with structural data that show that BI64 binds to an induced hydrophobic pocket at the base of CA-NTD.¹⁹ This pocket is located among α -helices 1, 2, 4, and 7 and is normally occupied by the aromatic side chain of Phe32 and His62 in the CA hexamer, pentamer, and monomer structures. Binding of BI64 repositions the flexible loop between helices 3 and 4 so that the loop conformation differs substantially from the apo-hexamer structure.¹⁶ All these changes would destabilize the CA-NTD–CTD interfaces that are required for the formation of higher-order assembled CA

species. Compared to BI64, PF74 has been studied more extensively using numerous biochemical, biophysical, and infectious cell-based assays.^{8,18,27,28,32} Furthermore, PF74 is considered as an important starting point for medicinal chemistry efforts in an attempt to develop a CA inhibitor suitable for human clinical testing. In 2014, at least three patents (WO2014/110296, WO2014/110297, and WO2014/110298) describing chemically optimized, highly potent compounds derived from PF74 were filed. Thus, understanding how PF74 binds and modulates CA is crucial for chemical optimization of PF74 and closely related compounds. Additionally, the availability of sensitive high-throughput assays to accurately measure compound potency and affinity like the assays described in our paper is equally important for the identification and optimization of PF74-based inhibitors. The data generated for PF74 using the label-free assays described in this study correlate very well with recently published work using structural and traditional binding assays such as ITC and sedimentation assays, which demonstrates that the principal inhibitory target for PF74 is the assembled CA and a binding location that encompasses an intermolecular CA-NTD–CTD interface. Binding of PF74 at this interface stabilizes CA in the assembled form and is consistent with our Epic assay-based studies showing that PF74 accelerates CA assembly and stabilizes preassembled CA tubes that are mainly composed of hexamers. The ability of PF74 to stabilize preassembled CA protein was confirmed using an ultracentrifugation (CA pelleting) assay and therefore further validates the Epic-based readout.^{28,32} However, this observation is not reproduced using isolated HIV-1 cores. Incubation of PF74 with isolated HIV-1 cores has been shown to have a destabilizing effect on the assembled CA using an ultracentrifugation assay.⁸ More recently, data were generated using an alternative assay that measures core stability during infection of cells over time and revealed PF74 stabilized CA hexamers but destabilized the mature CA.²⁸

We also used our label-free assays to characterize the interaction between CA and the cellular cofactor CPSF6. The binding affinity of the CPSF6-derived peptide, CPSF6_{313–327}, was significantly weaker than that of the small molecules used in this study, but the binding properties and the functional mechanism in the Epic assay indicate that CPSF6_{313–327} behaves like PF74 and suggests an overlapping binding site. Our results are consistent with recent comprehensive studies characterizing the binding interaction between CA and CPSF6_{313–327} that revealed the peptide preferentially binds to the hexameric CA form and the cocrystal structure of CPSF6_{313–327} bound to hexameric CA showed CPSF6 binds at the NTD–CTD interface between two monomers, which mirrors the binding site of PF74.^{27,28} Furthermore, competition experiments showed that PF74 inhibited binding of CPSF6_{313–327} to hexameric CA, suggesting PF74 is a competitive inhibitor of the CPSF6 cofactor.²⁷ From a drug discovery stand point, because PF74 occupies only a subset of the CPSF6-binding site it may provide an opportunity to synthesize a more potent PF74-based inhibitor that is suitable for clinical testing. Lastly, the assays described in our paper can also be used for the identification and characterization of compounds that target capsid proteins for other viral targets, specifically hepatitis B (HBV). Targeting HBV capsid as a therapeutic strategy to eliminate the virus is becoming the focus of intense research for small and large biotech companies. According to the World Health Organization, there are

~350 million people infected with HBV worldwide, and this is greater than the combined number of people infected with HIV (~35–40 million) and HCV (~170–200 million). Traditional high-throughput turbidity assays for measuring capsid assembly and disassembly cannot be used for HBV capsid because of the size and structure of the HBV capsid, and the assays described in this study could provide researchers with alternative platforms for identifying, characterizing, and optimizing druglike compounds for HBV capsid.

AUTHOR INFORMATION

Corresponding Author

*E-mail: Latesh.Lad@gilead.com. Telephone: (650) 522-2853. Fax: (650) 522-5166.

Notes

The authors declare no competing financial interest.

ACKNOWLEDGMENTS

We thank the associated support groups within Gilead Research that performed tasks in the generation of data reported herein. In addition, we gratefully acknowledge Stephanie Leavitt for technical help with ITC- and SPR-based experiments and data analysis. We also thank Sarah Wise, Annapurna Sapre, Jayshali Lad, and Leah Lad for encouragement and helpful discussions during the preparation of the manuscript.

REFERENCES

- (1) Smith, R. J., Okano, J. T., Kahn, J. S., Bodine, E. N., and Blower, S. (2010) Evolutionary dynamics of complex networks of HIV drug-resistant strains: The case of San Francisco. *Science* 327, 697–701.
- (2) Taiwo, B. (2009) Understanding transmitted HIV resistance through the experience in the USA. *Int. J. Infect. Dis.* 13, 552–559.
- (3) Prevelige, P. E., Jr. (2011) New approaches for antiviral targeting of HIV assembly. *J. Mol. Biol.* 410, 634–640.
- (4) Briggs, J. A., Simon, M. N., Gross, I., Kräusslich, H. G., Fuller, S. D., Vogt, V. M., and Johnson, M. C. (2004) The stoichiometry of Gag protein in HIV-1. *Nat. Struct. Mol. Biol.* 11, 672–675.
- (5) Forshey, B. M., von Schwedler, U., Sundquist, W. I., and Aiken, C. (2002) Formation of a human immunodeficiency virus type 1 core of optimal stability is crucial for viral replication. *J. Virol.* 76, 5667–5677.
- (6) Dismuke, D. J., and Aiken, C. (2006) Evidence for a functional link between uncoating of the human immunodeficiency virus type 1 core and nuclear import of the viral preintegration complex. *J. Virol.* 80, 3712–3720.
- (7) Ganser-Pornillos, B. K., von Schwedler, U. K., Stray, K. M., Aiken, C., and Sundquist, W. I. (2004) Assembly properties of the human immunodeficiency virus type 1 CA protein. *J. Virol.* 78, 2545–2552.
- (8) Shi, J., Zhou, J., Shah, V. B., Aiken, C., and Whitby, K. (2011) Small-molecule inhibition of human immunodeficiency virus type 1 infection by virus capsid destabilization. *J. Virol.* 85, 542–549.
- (9) Momany, C., Kovari, L. C., Prongay, A. J., Keller, W., Gitti, R. K., Lee, B. M., Goralenya, A. E., Tong, L., McClure, J., Ehrlich, L. S., Summers, M. F., Carter, C., and Rossmann, M. G. (1996) Crystal structure of dimeric HIV-1 capsid protein. *Nat. Struct. Mol. Biol.* 3, 763–770.
- (10) Berthet-Colominas, C., Monaco, S., Novelli, A., Sibai, G., Mallet, F., and Cusack, S. (1999) Head-to-tail dimers and interdomain flexibility revealed by the crystal structure of HIV-1 capsid protein (p24) complexed with a monoclonal antibody Fab. *EMBO J.* 18, 1124–1136.
- (11) Mortuza, G. B., Haire, L. F., Stevens, A., Smerdon, S. J., Stoye, J. P., and Taylor, I. A. (2004) High-resolution structure of a retroviral capsid hexameric amino-terminal domain. *Nature* 431, 481–485.
- (12) Ganser, B. K., Li, S., Klishko, V. Y., Finch, J. T., and Sundquist, W. I. (1999) Assembly and analysis of conical models for the HIV-1 core. *Science* 283, 80–83.
- (13) Li, S., Hill, C. P., Sundquist, W. I., and Finch, J. T. (2000) Image reconstructions of helical assemblies of the HIV-1 CA protein. *Nature* 407, 409–413.
- (14) Lanman, J., Lam, T. T., Barnes, S., Sakalian, M., Emmett, M. R., Marshall, A. G., and Prevelige, P. E. J. (2003) Identification of novel interactions in HIV-1 capsid protein assembly by high-resolution mass spectrometry. *J. Mol. Biol.* 325, 759–772.
- (15) Ganser-Pornillos, B. K., Cheng, A., and Yeager, M. (2007) Structure of full-length HIV-1 CA: A model for the mature capsid lattice. *Cell* 131, 70–79.
- (16) Pornillos, O., Ganser-Pornillos, B. K., Kelly, B. N., Hua, Y., Whitby, F. G., Stout, C. D., Sundquist, W. I., Hill, C. P., and Yeager, M. (2009) X-ray structures of the hexameric building block of the HIV capsid. *Cell* 137, 1282–1292.
- (17) Pornillos, O., Ganser-Pornillos, B. K., and Yeager, M. (2011) Atomic-level modelling of the HIV capsid. *Nature* 469, 424–427.
- (18) Blair, W. S., Pickford, C., Irving, S. L., Brown, D. G., Anderson, M., Bazin, R., Cao, J., Ciaramella, G., Isaacson, J., Jackson, L., Hunt, R., Kjerrstrom, A., Nieman, J. A., Patick, A. K., Perros, M., Scott, A. D., Whitby, K., Wu, H., and Butler, S. L. (2010) HIV capsid is a tractable target for small molecule therapeutic intervention. *PLoS Pathog.* 6, 1–10.
- (19) Lemke, C. T., Titolo, S., von Schwedler, U., Goudreau, N., Mercier, J. F., Wardrop, E., Faucher, A. M., Coulombe, R., Banik, S. S., Fader, L., Gagnon, A., Kawai, S. H., Rancourt, J., Tremblay, M., Yoakim, C., Simoneau, B., Archambault, J., Sundquist, W. I., and Mason, S. W. (2012) Distinct effects of two HIV-1 capsid assembly inhibitor families that bind the same site within the N-terminal domain of the viral CA protein. *J. Virol.* 86, 6643–6655.
- (20) Lanman, J., Sexton, J., Sakalian, M., and Prevelige, P. E., Jr. (2002) Kinetic analysis of the role of intersubunit interactions in human immunodeficiency virus type 1 capsid protein assembly in vitro. *J. Virol.* 76, 6900–6908.
- (21) Price, A. J., Fletcher, A. J., Schaller, T., Elliott, T., Lee, K., KewalRamani, V. N., Chin, J. W., Towers, G. J., and James, L. C. (2012) CPSF6 defines a conserved capsid interface that modulates HIV-1 replication. *PLoS Pathog.* 8, 1–14.
- (22) Ruepp, M. D., Aringhieri, C., Vivarelli, S., Cardinale, S., Paro, S., Schümperli, D., and Barabino, S. M. (2009) Mammalian pre-mRNA 3' end processing factor CF Im 68 functions in mRNA export. *Mol. Biol. Cell* 20, S211–S223.
- (23) Lee, K., Ambrose, Z., Martin, T. D., Oztop, I., Mulky, A., Julias, J. G., Vandegraaff, N., Baumann, J. G., Wang, R., Yuen, W., Takemura, T., Shelton, K., Taniuchi, I., Li, Y., Sodroski, J., Littman, D. R., Coffin, J. M., Hughes, S. H., Unutmaz, D., Engelman, A., and KewalRamani, V. N. (2010) Flexible use of nuclear import pathways by HIV-1. *Cell Host Microbe* 7, 221–233.
- (24) Hung, M., Niedziela-Majka, A., Jin, D., Wong, M., Leavitt, S., Brenda, K. M., Liu, X., and Sakowicz, R. (2013) Large-scale functional purification of recombinant HIV-1 capsid. *PLoS One* 8, 1–11.
- (25) Tsiang, M., Niedziela-Majka, A., Hung, M., Jin, D., Hu, E., Yant, S., Samuel, D., Liu, X., and Sakowicz, R. (2012) A trimer of dimers is the basic building block for human immunodeficiency virus-1 capsid assembly. *Biochemistry* 51, 4416–4428.
- (26) Gamble, T. R., Yoo, S., Vajdos, F. F., von Schwedler, U. K., Worthylake, D. K., Wang, H., McCutcheon, J. P., Sundquist, W. I., and Hill, C. P. (1997) Structure of the carboxyl-terminal dimerization domain of the HIV-1 capsid protein. *Science* 278, 849–853.
- (27) Price, A. J., Jacques, D. A., McEwan, W. A., Fletcher, A. J., Essig, S., Chin, J. W., Halambage, U. D., Aiken, C., and James, L. C. (2014) Host Cofactors and Pharmacologic Ligands Share an Essential Interface in HIV-1 Capsid That Is Lost upon Disassembly. *PLoS Pathog.* 10, 1–17.
- (28) Bhattacharya, A., Alam, S. L., Fricke, T., Zadrozny, K., Sedzicki, J., Taylor, A. B., Demeler, B., Pornillos, O., Ganser-Pornillos, B. K., Diaz-Griffero, F., Ivanov, D. N., and Yeager, M. (2014) Structural basis

of HIV-1 capsid recognition by PF74 and CPSF6. *Proc. Natl. Acad. Sci. U.S.A.* 111, 18625–18630.

(29) Rasaiyaah, J., Tan, C. P., Fletcher, A. J., Price, A. J., Blondeau, C., Hilditch, L., Jacques, D. A., Selwood, D. L., James, L. C., Noursadeghi, M., and Towers, G. J. (2013) HIV-1 evades innate immune recognition through specific cofactor recruitment. *Nature* 503, 402–405.

(30) Adamson, C. S., and Freed, E. O. (2010) Novel approaches to inhibiting HIV-1 replication. *Antiviral Res.* 85, 119–141.

(31) Mascarenhas, A. P., and Musier-Forsyth, K. (2009) The capsid protein of human immunodeficiency virus: Interactions of HIV-1 capsid with host protein factors. *FEBS J.* 276, 6118–6127.

(32) Fricke, T., Brandariz-Núñez, A., Wang, X., Smith, A. B. R., and Diaz-Griffero, F. (2013) Human cytosolic extracts stabilize the HIV-1 core. *J. Virol.* 87, 10587–10597.